Technical Note

Institution of MECHANICAL ENGINEERS
Journal of AEROSPACE ENGINEERING

Proc IMechE Part G:
J Aerospace Engineering
2023, Vol. 237(7) 1714–1724

DOI: 10.1177/09544100221133867
journals.sagepub.com/home/pig
Sage

Frequency modulation analysis of solar array using genetic algorithm

Rui Zhu[1] **and Dong Jiang**[2]

Abstract

In this paper, the optimal placement of prestress (OPP) is investigated for solar array frequency modulation using the genetic algorithm (GA). The purpose of OPP is to improve the solar array's fundamental frequency and prevent coupling resonance between the solar array and the microwave imager. Prestress is applied to a solar panel by the tension actuators. For optimization producers, the finite element model is used to analyze the prestress configuration problem, which can be converted into the number of programming decision constraints. The automatic interactive updating calculation between MATLAB and finite element software is realized by programming. The GA is used to optimize the solution. Region detection is used, and the bad individuals can be eliminated directly to avoid fitness calculation and effectively improve the optimization efficiency. Simulations are conducted for a solar panel with four arrays. Single-, two-, and three-plate optimizations are investigated. Four optimization parameters include the abscissa value, ordinate value, the laying direction of the actuator in the global coordinate system, and the prestress magnitude. Results demonstrate that the fundamental frequency reaches the maximum at a horizontal layout of prestress after the frequency modulation. The optimal solution is obtained when the prestress is placed in No.2, No.3, and No.4 plates.

Keywords

frequency modulation, genetic algorithm, prestress, actuators, solar array

Date received: 28 May 2022; revised: 25 August 2022; accepted: 14 September 2022

Introduction

Modern structural spacecraft usually carry large flexible appendages such as solar panels,[1] which are mainly composed of composite materials.[2] Due to the low damping of lightweight structures, the vibration attenuation time is long, which affects the normal operation of the structure.[3] Therefore, how to realize active control is of vital importance in spacecraft. The ideal dynamic characteristics can be obtained through the optimal distribution of actuators. The advantage of the optimal placement is not only to suppress the adverse response[4] but also to reduce the control energy requirements of the actuator.[5] In space engineering, a satellite is equipped with a microwave imager and a solar array. The imaging device has a specific rotation period. Several order frequencies of the solar array are close to the payload operating a frequency of the microwave imager, which can cause the coupling oscillation of the solar array's attitude. Natural frequencies can be obtained by system identification methods.[6–8] To ensure the operation of the spacecraft, it is necessary that avoiding the coupling resonance between the solar array and the microwave imager is implemented by frequency modulation.

Piezoelectric has been widely reported as a common device for active vibration control of flexible structures.[9,10] Many methods have been proposed to determine the optimal layout. Multiple optimization indicators[11] are investigated to fix up the placement of piezoelectric actuators on intelligent structures. In traditional analysis of active large flexible structures, numeric problems are caused by high-order computation. Therefore, the novel optimization method[12] is presented to overcome the defects above. The finite element method is utilized to discuss the active control performance of piezoelectric composite laminates,[13] and the simulated annealing method is proposed to reduce the structural amplitude and adjust the natural frequency of the structure. Moghaddam

[1] Institute of Flight System Dynamics, Technical University of Munich, Munich, Germany
[2] School of Mechanical and Electronic Engineering, Nanjing Forestry University, Nanjing, China

Corresponding author:
Dong Jiang, School of Mechanical and Electronic Engineering, Nanjing Forestry University, Nanjing, China.
Email: jiangdong@njfu.edu.cn

et al.[14] introduced a particle swarm optimization algorithm, successfully applied to simply supported slab under different loading conditions. Cao et al.[15] proposed a comprehensive learning particle swarm optimizer (CLPSO) embedded with local search (LS), and results show that this method has an overall higher convergence rate and accuracy. Bi et al.[16] proposed a partial computation offloading method to minimize the total energy consumed by SMDs and edge servers by jointly optimizing the offloading ratio of tasks, CPU speeds of SMDs, allocated bandwidth of available channels, and transmission power of each SMD in each time slot.

For practical optimization problems,[17–19] Yildiz et al.[20] compared the cuckoo search (CS) with other traditional optimization methods through a milling design problem, and the effectiveness of the proposed method is verified. The advantage of this method is that it generally has good global search performance, but sometimes it will fall into optimal local solution.[21] Sekhar et al.[22] and Teymourian et al.[23] have developed some improved CS algorithms to overcome the disadvantages above. Taking the reliability optimization problem of complex engineering as the research object, the accuracy and convergence of a new CS algorithm are verified.[24] Besides, GA as a common optimization algorithm is widely applied to the location optimization problem. Rao et al.[25] introduced the analysis steps and characteristics of GA, and illustrated the process through an example. An integer-real-encoded GA[26] is investigated to reduce the response of smart beams, and the vibration control is realized by arranging the position of the piezoelectric element reasonably. A novel implementation of the GA is proposed to improve the coverage of the sensor network for damage detection using guided waves.[27] The implementation allows the depiction of sensor locations with real values which is closer to the real-life situation. The optimal placement of the piezoelectric actuator on thin plates is discussed using integer coding GA,[28] and the input of the piezoelectric actuator is determined by the proposed controllability index. Bruant et al.[29] investigated the optimization problem of a double-objective function based on GA, and determined the number and optimal position of controllers. Based on the weighted processing technology,[30] the optimization problem of the uncertain model is transformed into a deterministic problem for processing, and the optimal solution is achieved by GA.

The existing methods mainly optimize the response feedback of the structure, while limited attention has been focused on the optimization for the inherent characteristics of the structure. To satisfy the dynamic characteristics of the structural design requirements, prestress is applied to the structure by tension actuators. For solar array frequency modulation, an optimization strategy based on a GA is utilized to determine the prestress's optimal placement. The framework of this paper is as follows: *The Problem formulation* introduces the Problem formulation about the coupling resonance between the solar array and the microwave imager. The GA for optimal prestress location is described in *The Optimization implementation using GA*. Numerical cases of the solar array are presented in *The Simulation and discussion*. *The Final* is a summary of this paper.

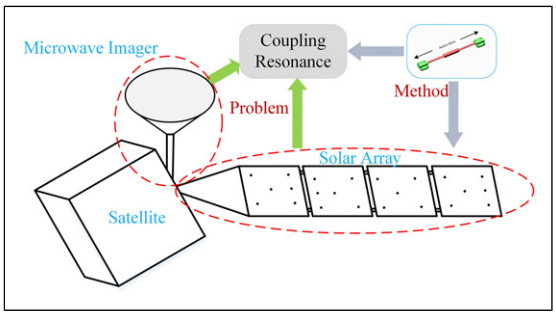

Figure 1. Problem of Solar panel.

Problem formulation

As shown in Figure 1, the satellite structure is mainly composed of a microwave imager and a solar array. The imaging device has a specific rotation period. Several order frequencies of the solar array may be close to the payload operating a frequency of the microwave imager, which can cause the coupling oscillation of the solar array's attitude and lead to structural damage.

The fundamental frequencies of the solar array can be analyzed by the finite element method. $M \in R^{n\times n}$ represents the mass matrix, where n is the degrees of freedom. $K \in R^{n\times n}$ is the stiffness matrix. The damping matrix is represented by the character C. The external force is F. x is the vibration displacement. The dynamic equation[31] of the solar panel is expressed as

$$M\ddot{x} + C\dot{x} + Kx = F \tag{1}$$

When the inherent dynamic characteristics of structures are investigated, the damping terms and external forces are not considered (C=0, F=0), and equation (1) is expressed as

$$M\ddot{x} + Kx = 0 \tag{2}$$

The solution of the equation can be set to $x=\boldsymbol{A}\sin(\omega t+\varphi)$, $\boldsymbol{A}$ is the vibration amplitude, ω is the circular frequency, t is the time, and φ is the initial phase, which is substituted into equation (2)

$$\left[K - \omega^2 M\right]A = 0 \tag{3}$$

The condition that the formula has a non-zero solution is

$$\left|K - \omega^2 M\right| = 0 \tag{4}$$

where ω is the natural frequency of the structure.

To avoid the coupling resonance between the solar array and the microwave imager, the prestress p is applied in the structure to adjust the structure frequency by actuators. The actuator is embedded in the construction, which can avoid the wingding problems of rope structures

$$M\ddot{x} + C\dot{x} + Kx = F + P \tag{5}$$

Since the solution of structural stiffness is geometrically nonlinear, the calculation process needs several iterations. In this case, the geometric equation becomes nonlinear, a quadratic derivative term is added based on the linear equation, and its tensor is expressed a

$$\varepsilon_{ij} = \frac{1}{2}\left(u_{i,j} + u_{j,i}\right) + \frac{1}{2}\left(u_{1,i} \times u_{1,j} + u_{2,i} \times u_{2,j} + u_{3,i} \times u_{3,j}\right) \quad (i,j = 1,2,3) \tag{6}$$

When the structure is subjected to prestress, the stress under vibration can be expressed as

$$\sigma = \sigma_p + \sigma_v \tag{7}$$

where σ_p is the prestress of the structure, and σ_v is the stress produced in the process of structural vibration. equation (6) and (7) are used to solve the strain energy of the structure, and the higher-order terms are omitted. The stiffness matrix of the fabric is obtained by the Hamilton principle[32]

$$K = K_L + K_{NL} \tag{8}$$

where K_L is a linear term of the stiffness matrix.[33] The term of the nonlinear stiffness matrix is represented by K_{NL}, called geometric stiffness. The expressions were

$$K_L = \int_V B_L^T D B_L dV \tag{9}$$

$$K_{NL} = \int_V B_{NL}^T D B_{NL} dV \tag{10}$$

where B_L is transformation matrices of linear strain vector ε and nodal displacement vector q. The abstract three-dimensional finite element is considered.[34] The linear strain vector is expressed by ε

$$\varepsilon = \left\{ \varepsilon_x \quad \varepsilon_y \quad \varepsilon_z \quad \gamma_{xy} \quad \gamma_{yz} \quad \gamma_{zx} \right\} \tag{11}$$

The nodal displacement vector is represented by q

$$q = \left\{ u_1 \quad v_1 \quad w_1 \quad u_2 \quad v_2 \quad w_2 \quad \cdots \right\} \tag{12}$$

Displacements at some point inside a finite element u can be determined with the use of nodal displacements q and shape functions $N_{i.}$

$$\begin{aligned} u &= \sum N_i u_i \\ v &= \sum N_i v_i \\ w &= \sum N_i w_i \end{aligned} \tag{13}$$

These relations can be rewritten in a matrix form as follows

$$\begin{aligned} u &= Nq \\ N &= \begin{bmatrix} N_1 & 0 & 0 & N_2 & \cdots \\ 0 & N_1 & 0 & 0 & \cdots \\ 0 & 0 & N_1 & 0 & \cdots \end{bmatrix} \end{aligned} \tag{14}$$

Strains can also be determined through displacements at nodal points

$$\begin{aligned} \varepsilon &= B_L q \\ B_L &= \begin{bmatrix} B_1 & B_2 & B_3 & \cdots \end{bmatrix} \end{aligned} \tag{15}$$

B_L can be obtained by differentiation of displacements expressed through shape functions and nodal displacements

$$B_i = \begin{bmatrix} \partial N_i/\partial x & 0 & 0 \\ 0 & \partial N_i/\partial y & 0 \\ 0 & 0 & \partial N_i/\partial z \\ \partial N_i/\partial y & \partial N_i/\partial x & 0 \\ 0 & \partial N_i/\partial z & \partial N_i/\partial y \\ \partial N_i/\partial z & 0 & \partial N_i/\partial x \end{bmatrix} \tag{16}$$

Similarly, B_{NL} reflects the relationship of the nonlinear strain vector and nodal displacement vector.[35] It can be expressed as

$$B_{NL} = AG \tag{17}$$

with A and G can be written

$$A = \begin{bmatrix} a_x^T & 0 & 0 \\ 0 & a_y^T & 0 \\ 0 & 0 & a_z^T \\ a_y^T & a_x^T & 0 \\ 0 & a_z^T & a_y^T \\ a_z^T & 0 & a_x^T \end{bmatrix} \tag{18}$$

with

$$a_i = \begin{bmatrix} \dfrac{\partial u}{\partial i} \\ \dfrac{\partial v}{\partial i} \\ \dfrac{\partial w}{\partial i} \end{bmatrix} = \begin{bmatrix} \dfrac{\partial N_1}{\partial i} I & \dfrac{\partial N_2}{\partial i} I & \cdots & \dfrac{\partial N_n}{\partial i} I \end{bmatrix} q \; i = x, y, z \tag{19}$$

and

$$G = \begin{bmatrix} \dfrac{\partial N_1}{\partial x} I & \dfrac{\partial N_2}{\partial x} I & \cdots & \dfrac{\partial N_n}{\partial x} I \\ \dfrac{\partial N_1}{\partial y} I & \dfrac{\partial N_2}{\partial y} I & \cdots & \dfrac{\partial N_n}{\partial y} I \\ \dfrac{\partial N_1}{\partial z} I & \dfrac{\partial N_2}{\partial z} I & \cdots & \dfrac{\partial N_n}{\partial z} I \end{bmatrix} \tag{20}$$

where I is the identity matrix.

Then additional stiffness matrix K_{NL} due to prestressed load can be expressed as

$$K_{NL} = \int_V G^T S G dV \tag{21}$$

where G has been shown in equation (20) and S is the initial element stress matrix due to prestressed load,[35] which can be expressed as

$$S = \begin{bmatrix} \sigma_x & \tau_{xy} & \tau_{xz} \\ \tau_{yx} & \sigma_y & \tau_{yz} \\ \tau_{zx} & \tau_{zy} & \sigma_z \end{bmatrix} \tag{22}$$

Considering the geometric nonlinearity, the prestress on the structure will cause the geometric stiffness of the additional nonlinear term of the stiffness matrix. Under the action of tensile stress, the stress matrix is positive, the geometric stiffness is also positive, and the overall stiffness increases; while under compressive stress, the overall stiffness decreases.

In solving dynamic problems, the stiffness matrix usually only has a linear term K_L, which cannot describe the change of structural stiffness caused by stress. When the geometric nonlinearity is considered, the prestress field inside the structure will make the stiffness matrix produce an additional nonlinear term (i.e., geometric stiffness K_{NL}), leading to structural stiffness and the natural frequencies will change.

Optimization implementation using GA

In this section, the basic theory of GA is introduced in detail. A GA is regarded as a random search technique. The right solution is determined by parameter search. Good results from the previous search can be obtained and accumulated automatically, and the subsequent search direction can be automatically determined. All alternatives can be considered as a population. Due to each individual's different characteristics, it can be used as an indicator of individual adaptability to the environment. The rule of survival of the fittest shows that individuals with better performance have a better chance to pass on characteristics to the next generation. If their offspring inherit each parent's best features, the probability of new individuals' survival is higher.

Genetic operation

This method is based on the random generation statistics of the population and mainly includes three steps:

Selection. The excellent individuals are selected from the current situation, and they are regarded as alternative fathers to generate the next individual. The principle is that individuals with strong adaptability have a high probability of contributing one or more offspring to the next generation. This step thoroughly explains Darwin's principle of survival of the fittest.

Crossover. Crossover operations are crucial in the method implementation process. Based on the individual characteristics of the parents, a new individual is generated through a crossover operation. This process illustrates the idea of information exchange.

Mutation. Every individual randomly in the population is generated. As the likelihood of mutation increased, some genes in the selected individuals changed. Generally speaking, the probability of gene mutation in biological species is relatively small.

The final population can often provide various design schemes, and designers can choose the most appropriate plan.

Optimal prestress location using GA

The automatic interactive updating calculation between MATLAB and finite element software is realized by programming, which provides an effective analysis method for complex engineering problems. The natural frequencies of the solar array are affected by the value and distribution of prestress. Therefore, the optimal selection of prestress position for optimal frequency is worth investigating. The positions and value of the prestress, as design variables are investigated. The main steps of the frequency modulation optimization method based on GA are as follows:

Step 1. Initial chromosomes are generated randomly, which depends on the number of prestress and population.
Step 2. Fitness is calculated for each chromosome,[36] which indicates the superiority or inferiority of an individual or solution. Through region detection, the bad individuals can be eliminated directly to avoid fitness calculation and effectively improve the optimization efficiency.
Step 3. Next-generation chromosomes are generated based on genetic operators.
Step 4. The maximum number of iterations is G. Repeat steps 2 and 3. The stop criterion of the algorithm is that the evolution algebra G reaches the upper limit. According to the best controllable value, the corresponding chromosome is determined as the optimal position of prestress.

In the process of optimization, prestress is applied by a tension actuator in Figure 2. Essentially, the opposite forces are applied to the structure's two nodes. Figure 3 illustrates the layout information of the prestress schematically. In this case, there are four optimization parameters. The first two design variables are the abscissa value (x_A) and the ordinate value (y_A) of point A. The third design variable is the laying direction of the actuator α, where the direction of 0° is consistent with the positive direction of the y-axis in

the global coordinate system. The angle is counterclockwise positive. Because of the limitation of the manufacturing process, the paving edge is selected in discrete numerical values. Therefore, the corresponding point B can be determined by

$$\begin{cases} x_B = x_A - l\sin\alpha \\ y_B = y_A + l\cos\alpha \end{cases} \tag{23}$$

where l represents the length of an actuator. The fourth design variable is the prestress value F.

Structural optimization problems include discrete and continuous variables. From a mathematical point of view, boundary constraints of design variables can be represented by

$$\begin{cases} x_A^L \le x_A \le x_A^U \\ y_A^L \le y_A \le y_A^U \\ \alpha \in T = \{\alpha_1, \alpha_2, \cdots, \alpha_k\} \\ f \in F = \{f_1, f_2, \cdots f_m\} \end{cases} \tag{24}$$

where x_A^L and x_A^U indicate the upper and lower bounds of variable x_A. y_A^L and y_A^U represent the upper and lower limits of variable y_A. T is a set of discrete numbers representing the attribution of an angular variable, including α_1, α_2,…,α_k. F is a set of distinct numbers representing the attribution of force variables. And F contains p optional values.

The optimal position is solved to maximize the structure's fundamental frequency by GA. A calculation file (*.bdf) containing prestress (tension actuator) based on Nastran software is generated. The GA is used to modify the calculation file and optimization parameters. The objective function is that the fundamental frequency reaches the maximum

$$J = min\left(\frac{\omega_0}{\omega_i}\right) \tag{25}$$

where ω_0 is the fundamental frequency of the structure, and ω_i is the optimized structure's fundamental frequency.

The implementation process of the above frequency modulation optimization method is visualized in Figure 4.

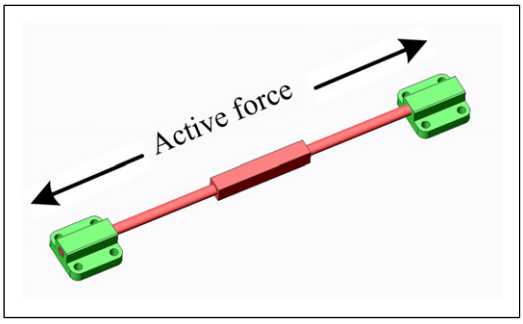

Figure 2. Tension actuators.

Simulation and discussion

It is assumed that the rotation period of the microwave imager is 1.7s (0.588 Hz). As shown in Figure 5, the solar array model consists of a scaffold and four arrays, and each panel is 640*400*3 mm. The distances between plates, arrays, and stents were all 5 cm; they are linked by hinges. The mechanical properties of the solar array are detailed in Table 1. The initial frequency of the structure is shown in Table 2. The first-order frequency (0.555 Hz) of the solar array is close to the microwave imaging frequency (0.588 Hz), which causes the coupling oscillation of the solar array's attitude. The expected result is that the solar array's natural frequency will not appear in the 0.470–0.705 Hz after the frequency modulation by using tension actuators. Plate No.1 is connected with the supporting rod, prestress force is considered to be applied to No.2, No.3, and No.4 plates. As shown in Figure 5, the finite element model of the solar array has a total of 10, 789 points and 10,381 elements. The plate is modeled with quadrilateral shell elements. The hinge is fixed to the sailboard, the RBE2 is used to simulate the bolt connection, and the six degrees of freedom are constrained to make it fixed. The connection between the plates is modeled by the CBUSH three-way spring-damper element. The bracket is modeled with CBAR elements.

Single plate optimization

Prestress is applied through tension actuators. For the convenience of explanation, it is preferred that actuators are installed on one plate. It is assumed that there are only two actuators in the No.2 plate, shown in Figure 6. The symmetrical arrangement is utilized. The middle green box (20×32 cm^2) is regarded as the search-space, where the actuator location can only be selected. The length of the actuator is l=12 cm. The location of actuators can be determined by two points (A, B).

In this case, there are four optimization parameters. The first two design variables are the abscissa value (X) and ordinate value (Y) of point A. The third design variable is the laying direction of the actuator (α). The set of desirable values is {0°, 90°, +45°, −45°}, where 0° is set in the same direction as the y-axis in the global coordinate system, and the angle is the counterclockwise positive.

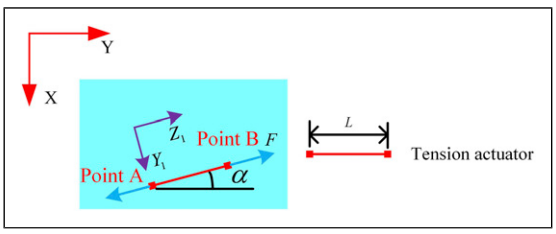

Figure 3. Schematic diagram of prestress.

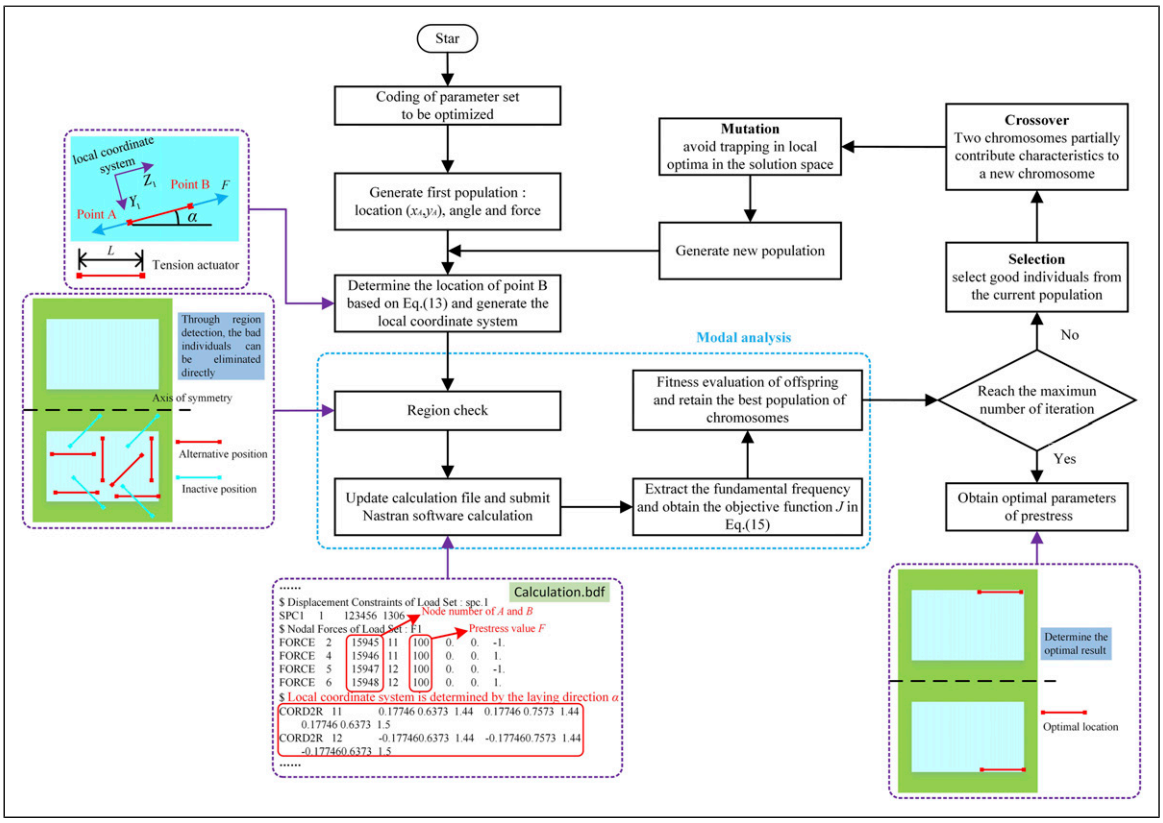

Figure 4. Flow chart of frequency modulation optimization method based on GA

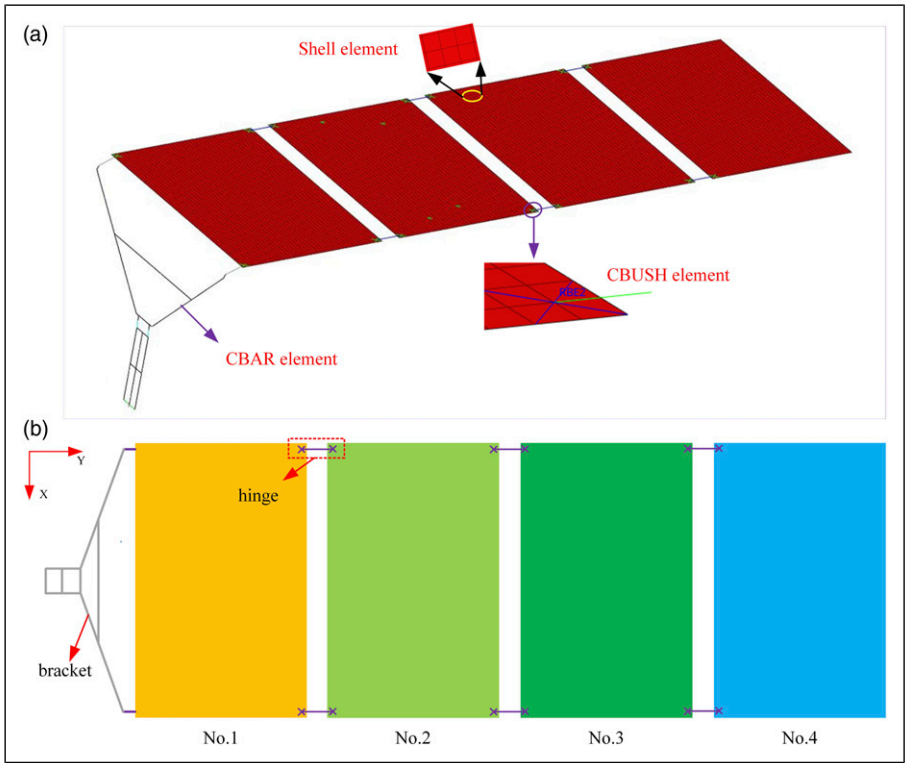

Figure 5. (a) Finite element model of solar array; (b) Schematic diagram of solar array.

Table 1. Characteristics of the solar array.

Elastic modulus (GPa)	Mass density (kg/m^3)	Poisson ratio
70	7800	0.3

Table 2. Nature frequencies of the initial structure.

Mode order	1	2	3	4	5	6
Nature frequency (Hz)	0.555	1.938	3.612	4.453	8.247	10.306

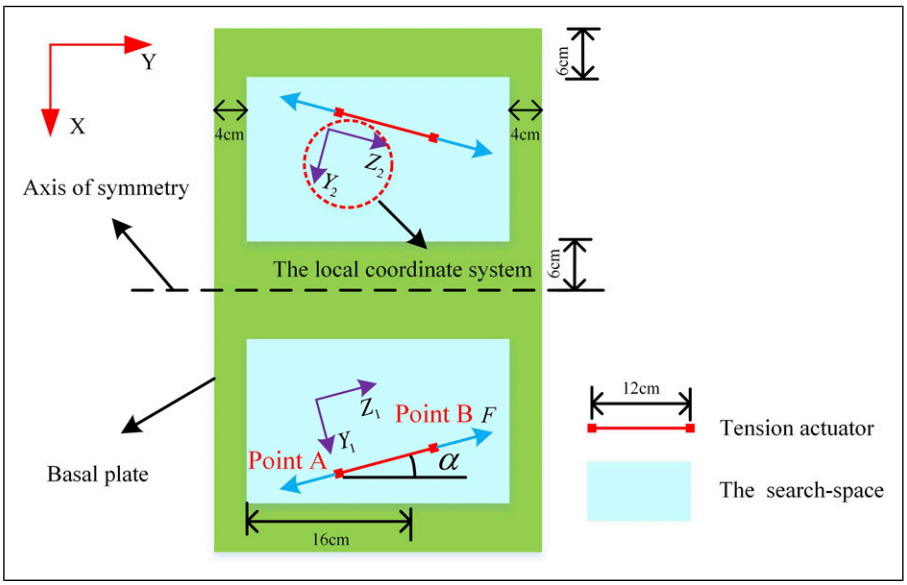

Figure 6. Schematic diagram of prestress.

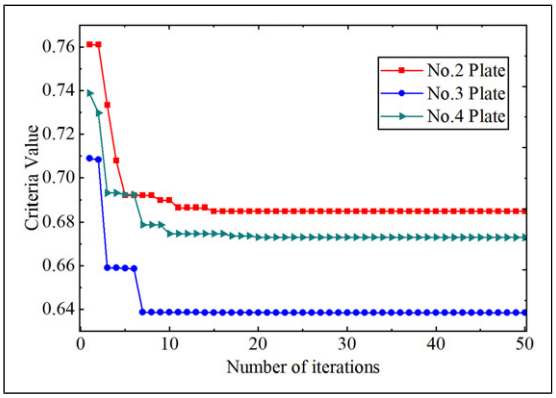

Figure 7. The convergence of GA in one plate optimization.

The fourth design variable is the prestress value F, and the set of desirable value ranges from 50N to 400N with an interval of 5. The prestress value needs to be modified, and the corresponding local coordinate system needs to be established in the Calculation.bdf file.

Initialize each particle $(x_A, y_A)$with a random position in the search-space for every plate

$$\begin{cases} x_A^2 \in [0.06, 0.26] \\ y_A^2 \in [0.49, 0.81] \end{cases} \text{for No.2 plate}$$
$$\begin{cases} x_A^3 \in [0.06, 0.26] \\ y_A^3 \in [0.94, 1.26] \end{cases} \text{for No.3 plate} \quad (26)$$
$$\begin{cases} x_A^4 \in [0.06, 0.26] \\ y_A^4 \in [1.39, 1.71] \end{cases} \text{for No.4 plate}$$

Meanwhile, the corresponding constraint is that point B must be in the search-space

$$\begin{cases} 0.06 \le x_B^2 \le 0.26 \\ 0.49 \le y_B^2 \le 0.81 \end{cases} \text{for No.2 plate}$$
$$\begin{cases} 0.06 \le x_B^3 \le 0.26 \\ 0.94 \le y_B^3 \le 1.26 \end{cases} \text{for No.3 plate} \quad (27)$$
$$\begin{cases} 0.06 \le x_B^4 \le 0.26 \\ 1.39 \le y_B^4 \le 1.71 \end{cases} \text{for No.4 plate}$$

If it goes beyond that range, the actuator will go beyond the search-space and not meet the setup

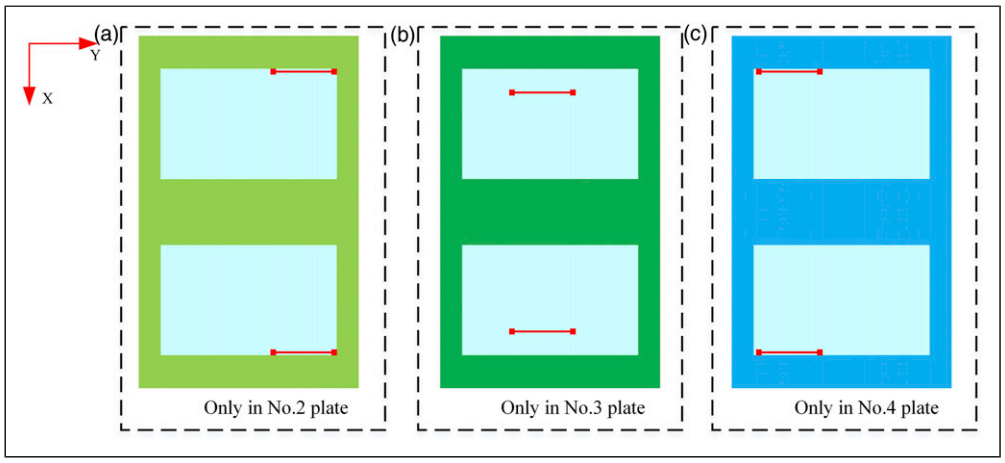

Figure 8. Optimal location of actuators in one plate optimization.

Table 3. Optimal parameters and results optimal of one plate

Case description	Point A				Optimization Value	Initial 1st model frequency/Hz	Optimized 1st model frequency/Hz
	X/m	Y/m	F/N	Angle			
Case 1 No.2 plate	0.260	0.688	400	0	0.685	0.555	0.810
Case 2 No.3 plate	0.222	1.026	400	0	0.638	0.555	0.869
Case 3 No.4 plate	0.260	1.395	400	0	0.673	0.555	0.825

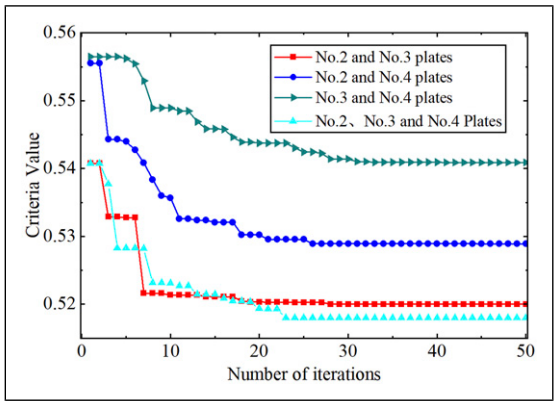

Figure 9. The convergence of GA in multi-plates.

requirements. The optimal placement of an actuator on a solar plate has been found by the frequency modulation optimization method. The convergences of the fitness function with a generation number as obtained are shown in Figure 7. The optimal location of actuators is shown in Figure 8. Optimal parameters and results optimal of one plate are given in Table 3. Results show that the optimal location is at the side of the search-space in Case 1 and Case 3. Frequency shifts identified in the numerical result are affected by structure deformation which affects stress stiffness matrices of prestressed structure. When prestress is applied near the middle surface of the structure, it produces much smaller deformation and frequency shifts stay very small.[33] Nevertheless, the optimal position is not at the edge of search-space in Case 2. The fundamental frequency reaches a maximum at α=0° and F=400N. All three cases ensure that there is no modal order in the frequency band (0.470–0.705 Hz). In the single-plate optimization, prestress is loaded on the No.3 plate, and the fundamental frequency (0.869 Hz) is optimal.

Multi-plates optimization

The arrangement of the pre-tightening force on multi-plates is considered. Four cases are carried out. The convergences of the fitness function with a generation number as obtained are shown in Figure 9. The optimal placement on a solar plate is shown in Figure 10, Figure 11, Figure 12, and Figure 13 based on the proposed method. Optimal parameters and results optimal of multi-plates are given in Table 4. Results show that the optimal location is at the edge of search-space in Case 5 and Case 6. Nevertheless, the optimal placement is not all at the edge of the search-space in Case 4 and Case 7. For multi-plates optimization, the fundamental frequency reaches a maximum at α=0° and F=400N, and there is no modal order in the frequency band (0.470–0.705 Hz), which verifies the effectiveness of frequency modulation. The

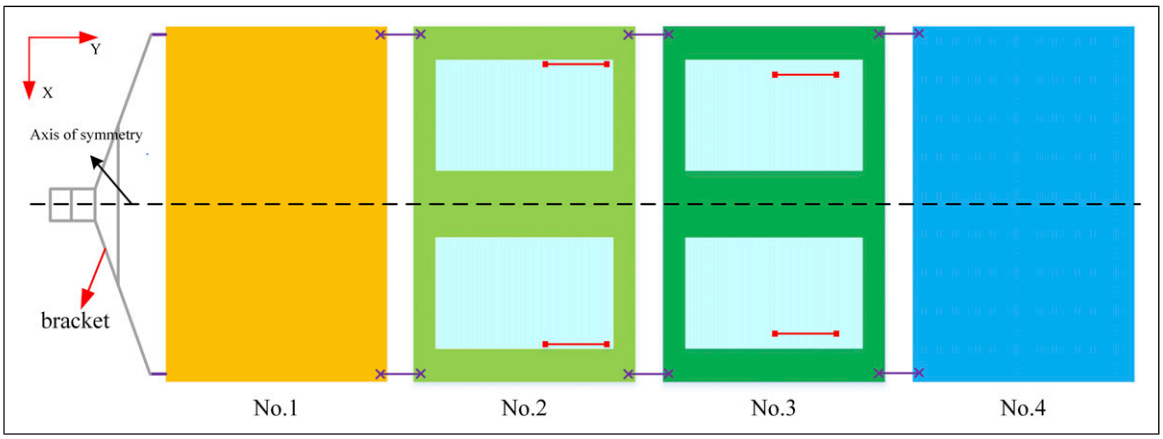

Figure 10. Results of two plates optimization (No.2 plate and No.3 plate).

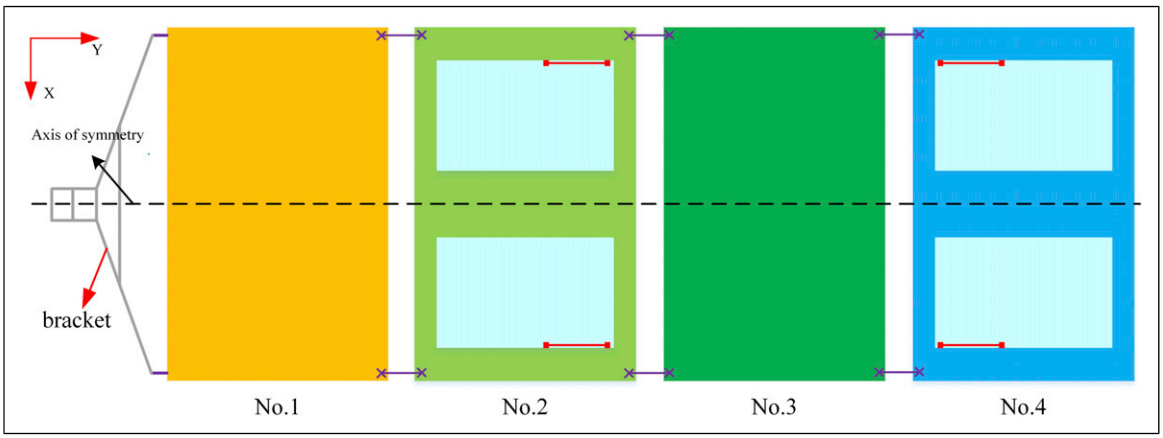

Figure 11. Results of two plates optimization (No.2 plate and No.4 plate).

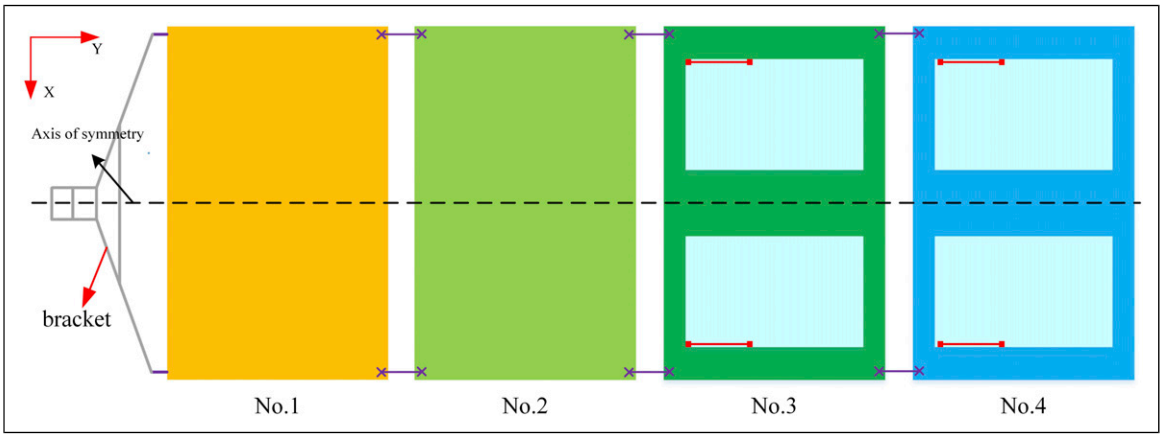

Figure 12. Results of two plates optimization (No.3 plate and No.4 plate).

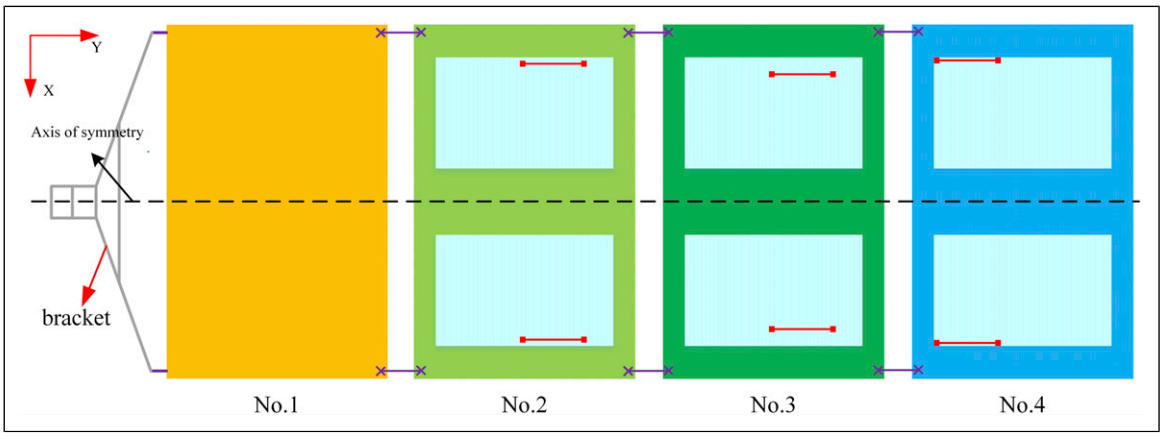

Figure 13. Results of three plates optimization (No.2 plate, No.3 plate, and No.4 plate).

Table 4. Optimal parameters and results optimal of multi-plates.

Case description		Point A				Optimization Value	Initial 1st model frequency/Hz	Optimized 1st model frequency/Hz
		X/m	Y/m	F/N	Angle			
Case 4	No.2 plate	0.257	0.683	400	0	0.520	0.555	1.067
	No.3 plate	0.238	1.097	400	0			
Case 5	No.2 plate	0.260	0.683	400	0	0.529	0.555	1.049
	No.4 plate	0.260	1.395	400	0			
Case 6	No.3 plate	0.260	0.940	400	0	0.541	0.555	1.026
	No.4 plate	0.260	1.395	400	0			
Case 7	No.2 plate	0.254	0.642	400	0	0.518	0.555	1.069
	No.3 plate	0.235	1.092	400	0			
	No.4 plate	0.260	1.390	400	0			

prestress is loaded in Case 7, and the fundamental frequency (1.069 Hz) is optimal.

Conclusion

An effective means of preventing coupling resonance between a solar array and a microwave imager is to improve the solar array's fundamental frequency by prestress. In this study, a frequency modulation optimization method based on GA was used to search the OPP in the solar array. Prestress was applied using tension actuators. The automatic interactive updating calculation between MATLAB and finite element software is realized by programming, which provides an effective analysis method for complex engineering problems. Through region detection, the bad individuals can be eliminated directly to avoid fitness calculation and effectively improve optimization efficiency. Numerical simulations were performed for the solar array with four arrays. It was assumed that prestress could be applied on No.2–4 plate, and single-, two-, and three-plate optimizations were investigated. The optimal placement illustrates that the solar array's fundamental frequency reaches the maximum at a horizontal layout of prestress. In all cases, the solar array's natural frequency does not appear in the 0.470–0.705 Hz after the frequency modulation by using tension actuators. The fundamental frequency (1.069 Hz) was optimal in Case 7. Results show that the proposed method can effectively avoid the coupling resonance between the solar array and the microwave imager.

Declaration of Conflicting Interests

The author(s) declared no potential conflicts of interest with respect to the research, authorship, and/or publication of this article.

Funding

The author(s) received no financial support for the research, authorship, and/or publication of this article.

ORCID iD

Rui Zhu https://orcid.org/0000-0001-8873-7098

References

1. Song G and Agrawal BN. Vibration suppression of flexible spacecraft during attitude control. *Acta Astronautica* 2001; 2(49): 73–83.
2. Jiang D, Li Y, Fei Q, et al. Prediction of uncertain elastic parameters of a braided composite. *Compos Structures* 2015; 126: 123–131.
3. Chen D, Zheng S and Wang H. GA based LQR vibration wireless control of laminated plate using photostrictive actuators. *Earthquake Eng Eng Vibration* 2012; 11(1): 83–90.

4. Cao Z, Fei Q, Jiang D, et al. Substructure-based model updating using residual flexibility mixed-boundary method. *J Mech Sci Technology* 2017; 31(2): 759–769.
5. Yang B, Miao J, Fan Z, et al. Modified cuckoo search algorithm for the optimal placement of actuators problem. *Appl Soft Comput* 2018; 67: 48–60.
6. Zhu R, Fei Q, Jiang D, et al. Identification of nonlinear stiffness and damping parameters using a hybrid approach. *AIAA J* 2021; 59(11): 4686–4695.
7. Zhu R, Fei Q, Jiang D, et al. Bayesian model selection in nonlinear subspace identification. *AIAA J* 2022; 60(1): 92–101.
8. Zhu R, Marchesiello S, Anastasio D, et al. Nonlinear system identification of a double-well Duffing oscillator with position-dependent friction. *Nonlinear Dyn* 2022; 108: 1–16.
9. Zhu R, Fei Q, Jiang D, et al. Removing mass loading effects of multi-transducers using Sherman-Morrison-Woodbury formula in modal test. *Aerospace Sci Technology* 2019; 93: 105241.
10. Zhu R, Fei Q, Jiang D, et al. Using Sherman–Morrison theory to remove the coupled effects of multi-transducers in vibration test. *Proc Inst Mech Eng G: J Aerospace Eng* 2019; 233(4): 1364–1376.
11. Gupta V, Manu S and Nagesh T. Optimization criteria for optimal placement of piezoelectric sensors and actuators on a smart structure: a technical review. *J Intell Mater Syst Structres* 2010; 21: 1227–1243.
12. Nestorović T and Trajkov M. Optimal actuator and sensor placement based on balanced reduced models. *Mech Syst Signal Process* 2013; 36(2): 271–289.
13. Simões Moita JM, Franco Correia VM, Martins PG, et al. Optimal design in vibration control of adaptive structures using a simulated annealing algorithm. *Compos Structures* 2006; 75(1–4): 79–87.
14. Moghaddam JJ and Bagheri A. A novel stable deviation quantum-behaved particle swarm optimization to optimal piezoelectric actuator and sensor location for active vibration control. *Proc Inst Mech Eng J Syst Control Eng* 2015; 229(6): 485–494.
15. Cao Y, Zhang H, Li W, et al. Comprehensive learning particle swarm optimization algorithm with local search for multimodal functions. *IEEE Trans Evol Comput* 2019; 23(4): 718–731.
16. Bi J, Yuan H, Duanmu S, et al. Energy-optimized partial computation offloading in mobile-edge computing with genetic simulated-annealing-based particle swarm optimization. *IEEE Internet Things J* 2020; 8(5): 3774–3785.
17. Guo G, Zhao Y, Su W, et al. Topology optimization of thin-walled cross section using moving morphable components approach. *Struct Multidisciplinary Optimization* 2021; 1: 1–18.
18. Zhu R, Fei QG, Jiang D, et al. Dynamic sensitivity analysis based on Sherman–Morrison–Woodbury formula. *AIAA J* 2019; 57(11): 4992–5001.
19. Ma Y, Chen R, Bai J, et al. Shape optimization of thin-walled cross section for automobile body considering stamping cost, manufacturability and structural stiffness. *Int J Automotive Technology* 2020; 21(2): 503–512.
20. Yildiz AR. Cuckoo search algorithm for the selection of optimal machining parameters in milling operations. *Int J Adv Manufacturing Technology* 2013; 64(1–4): 55–61.
21. Mohanty PK and Parhi DR. Optimal path planning for a mobile robot using cuckoo search algorithm. *J Exp Theor Artif Intelligence* 2016; 1–2(28): 35–52.
22. Sekhar P and Mohanty S. An enhanced cuckoo search algorithm based contingency constrained economic load dispatch for security enhancement. *Int J Electr Power Energ Syst* 2016; 75: 303–310.
23. Teymourian E, Kayvanfar V, Komaki G, et al. Enhanced intelligent water drops and cuckoo search algorithms for solving the capacitated vehicle routing problem. *Inf Sci* 2016; 334–335: 354–378.
24. Valian E, Tavakoli S, Mohanna S, et al. Improved cuckoo search for reliability optimization problems. *Comput Ind Eng* 2013; 64(1): 459–468.
25. Rao SS, Pan TS and Venkayya VB. Optimal placement of actuators in actively controlled structures using GAs. *AIAA J* 1991; 29(6): 942–943.
26. Yang Y, Jin Z and Kiong Soh C. Integrated optimal design of vibration control system for smart beams using GAs. *J Sound Vibration* 2005; 282(3–5): 1293–1307.
27. Soman R and Malinowski P. A real-valued genetic algorithm for optimization of sensor placement for guided wave-based structural health monitoring. *J Sensors* 2019; 2019: 1–10.
28. Vashist SK and Chhabra D. *Optimal placement of piezoelectric actuators on plate structures for active vibration control using GA*. SPIE, 2014.
29. Bruant I, Gallimard L and Nikoukar S. Optimization of piezoelectric sensors location and number using a GA. *Mech Adv Mater Structures* 2011; 18(7): 469–475.
30. Li Y, Wang X, Huang R, et al. Actuator placement robust optimization for vibration control system with interval parameters. *Aerospace Sci Technology* 2015; 45: 88–98.
31. Hu H. *Vibration mechanics: a research-oriented tutorial*. singapor: Springer verlag, 2022.
32. Liu Y, Tang K and Joneja A. Modeling dynamic developable meshes by the Hamilton principle. *Computer-Aided Des* 2007; 39(9): 719–731.
33. Orlowska A, Graczykowski C and Adam G. The effect of prestress force magnitude on the natural bending frequencies of the eccentrically prestressed glass fibre reinforced polymer composite beams. *J Compos Mater* 2018; 5215: 2115–2128.
34. Nikishkov GP. *Introduction to the finite element method*. University of Aizu, 2004, pp. 1–70.
35. Yang S and Yang Q. Geometrically nonlinear random vibration responses of composite plates subjected to acoustic excitation. *AIAA J* 2018; 56(7): 2827–2839.
36. Baker JE. Adaptive selection methods for genetic algorithms. *Proc Int Conf Genet algorithms their Appl* 1985; 1.